Review Article

BIOMEDICAL Journal of Scientific & Technical Research

ISSN: 2574 -1241

DOI: 10.26717/BJSTR.2026.66.010286

# Estimates of the Impact of Meteor Showers on Ultraviolet Radiation and Blood Markers

**AV Tertyshnikov***

*Institute of Applied Geophysics, Moscow, Russia*

***Corresponding author:** AV Tertyshnikoy, Institute of Applied Geophysics, 9 Rostokinskaya St., Moscow, Russia

**ARTICLE INFO**

**Received:** June 15, 2026

**Published:** July 06, 2026

**Citation:** AV Tertyshnikov. Estimates of the Impact of Meteor Showers on Ultraviolet Radiation and Blood Markers. Biomed J Sci & Tech Res 66(1)-2026. BJSTR. MS.ID.010286.

**ABSTRACT**

An interaction between solar ultraviolet radiation and meteoric dust has been established. The particle sizes of meteoric dust correspond to the wavelength range of solar ultraviolet radiation. Blood samples from the St. Petersburg Clinical Hospital for 2000-2001 were used to test this effect. Changes in the morphology of the spectral-temporal characteristics of the erythrocyte sedimentation rate (ESR), leukocyte counts, and lymphocyte counts were observed relative to the dates of strong meteor showers with dominant cycles of 3-4 and 6-7 days.

**Keywords:** Meteor Showers; Ultraviolet Radiation; Blood Markers; Generalized Profiles; Leukocytes; Lymphocytes; Eryth-Rocytes

## Introduction

One of the mechanisms by which heliogeophysical activity influences social activity may be related to the regulation of solar ultraviolet variations. This was demonstrated in (Tertyshnikov [1]) for the extreme ultraviolet maxima of strong meteor showers. Attention to the ultraviolet range is due to its comparability with the particle sizes of meteoric and cosmic dust. Variations in the density of meteoric dust in meteor showers, as one of the characteristics of meteoric material models in space, manifest themselves in variations in solar ultraviolet. Ground-based measurements of solar ultraviolet intensity were conducted at the Russian Antarctic Station Novolaz-arevskaya using two instruments: the UFI-1 Ultraviolet Meter (Ryabinin, 2006) and the AvaSpec-2048 Spectropho-tometer (Spectrometer, 2007). The UFI-1 device records the integrated ultraviolet radiation power in the erythemal activity range (297-330 nm). In its measuring circuit, solar radiation passes through a quartz hemispherical cap and a fluoroplastic diffuser onto a photodiode. The photodiode current is amplified by a preamplifier and converted into a digital signal by an analog-to-digital controller. The photocurrent, amplification parameters, and internal temperature are transmitted to the computer input via a USB cable. A heater maintains the internal temperature of the measuring unit within 20±2°C. The recorded power level is limited to 450 mW/m2. The device's measurement error is up to 20% for external temperatures of ±50°C. The AvaSpec-2048 fiber optic spectrometer allows for the measurement of ultraviolet radiation power across multiple wavelengths. It was used at Novolazarevskaya, including as a backup for measurements by the UFI-1 device. Measurements revealed an increase in the recorded intensity of solar ultraviolet radiation during the peaks of strong meteor showers (Tertyshnikov [1]). Taking into account the modulation of variations in solar ultraviolet intensity on the dates of strong meteor showers, the effect of a "natural germicidal lamp" can be diagnosed, for example, in blood characteristics. The influence of solar ultraviolet radiation on blood characteristics is discussed in (Shapovalov, et al. [2-5]).

## Experimental Design

To diagnose the effect of increased solar ultraviolet radiation on blood markers, strong meteor showers with peak dates from (Space Data, 2024) were used. The meteor shower selection criterion was a zenith hourly rate (ZHR) of at least 5 meteors per hour above the potential observer. The list of events included the following showers: January 3, February 8 and 24, March 14, June 7, June 19, July 30, August 6, August 13, September 1, September 9, October 21, November 17, and December 7 and 14. The experiment utilized blood samples from the St. Petersburg Clinical Hospital from May 28, 2000, to March 20, 2001, excluding July, on national holidays, and, to some extent, on weekends. For blood markers, the average values from the following 24-hour tests were used:

1) Erythrocyte sedimentation rate (ESR)
2) Lymphocyte count, and
3) Leukocyte count.

Between five and 15 blood tests were performed per day. Uncertainty in the health status of those undergoing the tests dictates the primary focus on assessing the dispersion of markers and their ordering on the generalized date of a strong meteor shower. For this purpose, the "generalized portrait" method (Tertyshnikov [5]) was used within an interval of ±10 days from the dates of strong meteor shower maxima, and the fast Fourier transform method was used, taking into account the small amplitude of the expected changes in blood markers.

## Analysis of Results

Figure 1a presents estimates of the standard deviation and coefficient of variation of the average daily erythrocyte sedimentation rate (ESR) estimates. Figure 1b shows the third and fourth moments of the distribution of the averaged ESR series. The vertical arrow indicates the day with the date of the strong meteor shower maximum. The ESR marker allows one to assess the presence of inflammation and other pathological changes in the body. In-creased amplitudes of variation in the obtained estimates are noticeable in the interval from -6 to +9 days from the date of the strong meteor shower's peak. However, on the peak date, with elevated solar ultraviolet radiation, variations are minimal, and the marker level returns to normal. The average ESR estimate on the date of the strong meteor shower was 5.2 mm/hour, compared to the normal range of 2–10 mm/hour for men and 2–15 mm/hour for women. ESR values on the -2 and +2 day dates are 60% higher than on the date of the strong meteor shower's maximum. On the date of strong meteor shower maxima, the kurtosis coefficient of the average daily ESR marker is negative (Figure 1b), which corresponds to a uniform distribution. Figure 1 shows a noticeable cyclicity, which is evident in the morphology of the spectral-temporal amplitudegrams calculated using the fast Fourier transform for a number of average daily ESR markers (Figure 2). Using spectral-temporal analysis allows us to diagnose subtle effects in variations in natural noise. A 16-day sliding window was used to construct the amplitudegram. The calculated amplitudegram was assigned to the middle of this window. Amplitude gradations are color-coded. Dominant cyclicity is evident in the increased amplitudes of the 4- and 7-day periods. From the date of the strong meteor shower maximum (day 0), their amplitude increases, and decreases during the intermediate periods. To compare changes across different periods, the calculated amplitudes of each period in Figure 2 were normalized relative to the minimum and maximum amplitude values of the period in the considered interval from -3 days to +5 days. The spectral-temporal distribution of the normalized amplitudes in Figure 2 is shown in Figure 3, which also uses color coding for the amplitude gradations.

Normalizing the amplitudes in each period improved the visibility of changes in the spectrum's morphology after the strong meteor shower's maximum, as well as the activity of the 3- 4 and 6- 7 day periods. The low-frequency contribution increases almost a week after the strong meteor shower's maximum. The power of the 2-day period decreases. The change in the average daily marker "leukocytes" is shown in Figure 4. Leukocytes are blood cells that provide immune protection, produce antibodies, and destroy foreign agents and dead or mutated cells. The normal level of leukocytes in the blood for adults should be (0.4-0.9)×1010/L. The level of the average daily "leukocytes" marker is below the average values within ±10 days from the date of the meteor shower's maximum and is elevated on the -3$^{rd}$ day and on the +4$^{th}$ day. Dominant periodicities of 3-4 and 7 days are also evident. Variations in average daily markers for leukocytes are ordered based on the excess coefficient, occurring at most 24 hours after the date of meteor shower maxima. The signal is strong, extending beyond the 95% confidence interval of the analyzed three-week series and corresponding to normal distribution levels, confirming the ordering effect of variations in the analyzed marker and immune system activation. Changes in the average daily marker "lymphocytes" (Figure 5) are largely similar to the estimates for leukocytes. Lymphocytes (blood cells that participate in the formation of the immune defense) are a type of leukocyte. The estimate of the average daily "lymphocyte" marker on the date of the strong meteor shower maximum is lower than the average values in the analyzed time period. Local maxima appear approximately a day later than for leukocytes. Dominant periodicities of 3-4 and 7 days are also present. A strong signal of ordering in the variations of average daily markers for lymphocytes is greatest on the day following the maxima of strong meteor showers, indicating activation of the immune system. The main function of lymphocytes is to recognize and destroy foreign agents in the body, primarily infectious pathogens and damaged cells.

 **DOI:** 10.26717/BJSTR.2026.66.010286

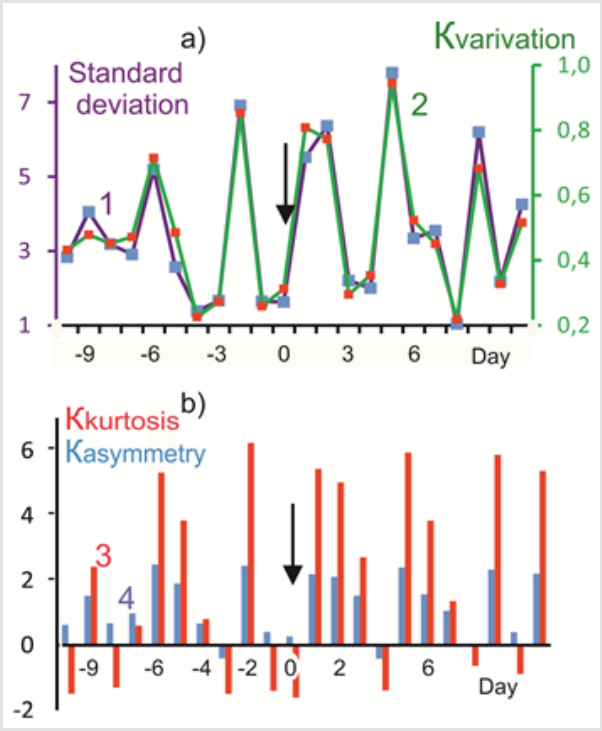


**Note:** The vertical arrow indicates the date of the strong meteor shower's peak.

Figure 1: Variations in average daily erythrocyte sedimentation rate estimates:

(a)

(1) Estimates of the standard deviation and

(2) The coefficient of variation

(b)

(3) The fourth and

(4) Third moments of the distribution of the averaged ESR series.

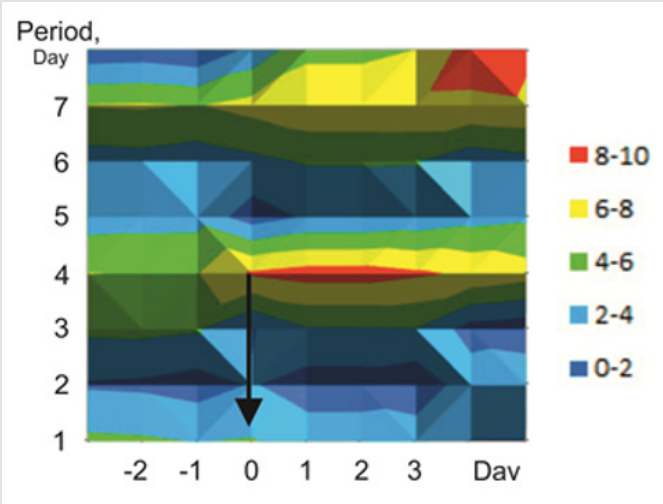


**Note:** The vertical arrow indicates the date of the strong meteor shower maximum.

**Figure 2:** Spectral-temporal distribution of the amplitudes of the averaged series of daily average ESR marker estimates.

**DOI:** 10.26717/BJSTR.2026.66.010286

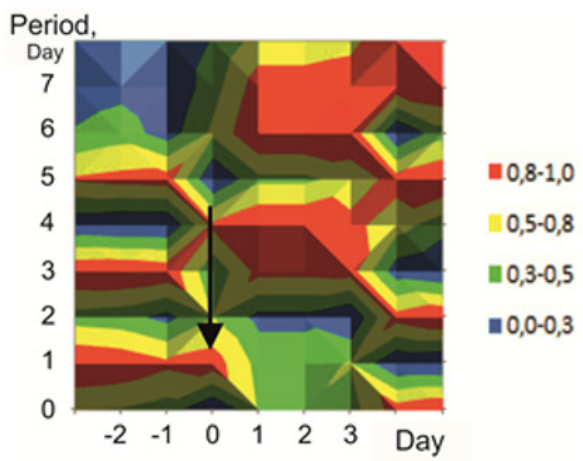


Note: The vertical arrow indicates the date of the strong meteor shower's maximum.

**Figure 3:** Distribution of normalized amplitude traces for Figure 2.

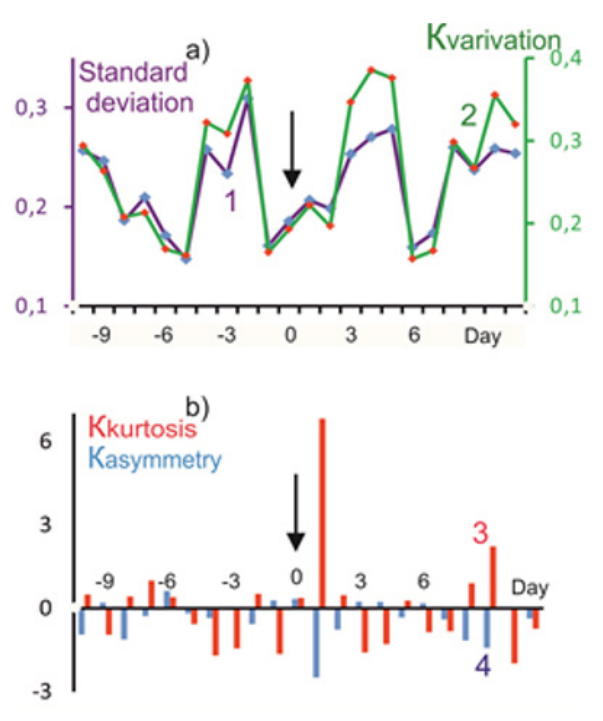


Note: The vertical arrow indicates the date of the strong meteor shower's maximum.

**Figure 4:** Variations in average daily estimates of the "leukocytes" marker:

(a)

(1) Estimates of the standard deviation and

(2) The coefficient of variation

(b)

(3) The fourth and

(4) Third

Moments of the distribution of the average series.

 **DOI:** 10.26717/BJSTR.2026.66.010286

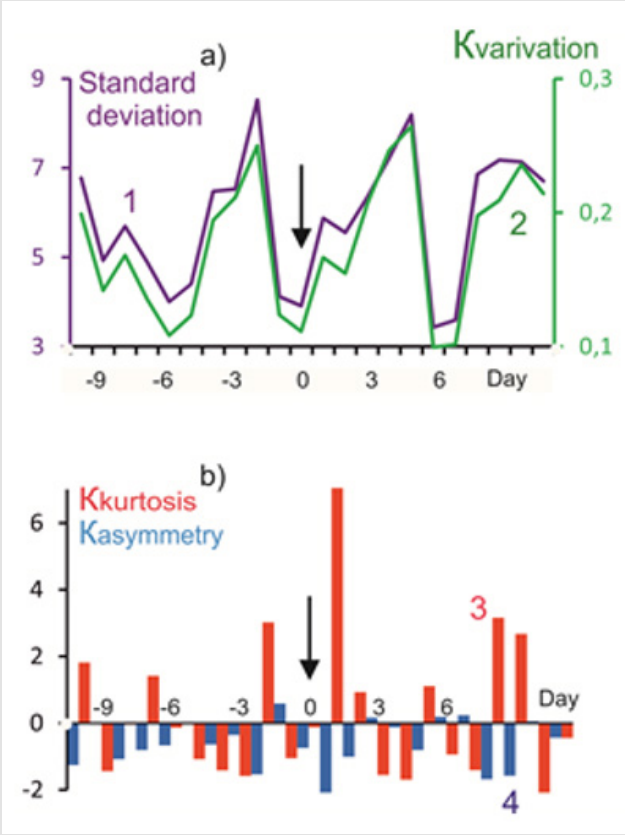


Note: The vertical arrow indicates the date of the strong meteor shower maximum.

**Figure 5:** Variations in the average daily estimates of the "lymphocyte" marker:

(a)

(1) Estimates of the standard deviation and

(2) The coefficient of variation

(b)

(3) The fourth and

(4) Third

Moments of the distribution of the averaged series.

## Discussion

The temporal correlation between the weak impact of meteor shower density variations on the upper atmosphere and changes in blood markers necessitates a search for possible mechanisms of interaction. These may include changes in atmospheric conductivity due to meteoric dust, an increase in solar ultraviolet radiation during the meteor shower's peak, the influence of solar ultraviolet radiation on pathogenic processes, and the manifestation of meteor shower density variations in the solar ultraviolet flux. Meteoric matter distribution models (GOST, et al. [6,7]) do not take into account meteor shower density variations, including those in the upper atmosphere. The first model is designed to calculate the spatial distribution of meteoric material in the ecliptic plane with particle masses of 10–6 ... 102 g at distances from the Earth's surface up to ~1,000,000 km, and meteoroids with masses of 10–9 ... 10–6 g at distances of 200–1000 km. Moreover, the velocities of meteoroids with masses up to 10–6 g relative to the Earth are assumed to be 20 km/s (Mironov [8]). In the sub-sequent development of meteoric material distribution models, priority was given to space debris models (GOST [9]), which require special consideration of dust from the incineration of Starlink satellites. The distribution of me-teoric dust from the Earth's surface to the exosphere, mesosphere, and stratosphere also remains unstudied. NASA and ESA regularly update their working versions of existing meteoroid models, which are used in the design of space-craft and the planning of various space missions. However, even these models ignore the range of up to 0.1 astronomical units from Earth (Wiegert [10]), although there is a selection of meteoric dust particles due to the ballistic braking of meteoric dust particles: as the mass and size of

dust particles decreases, their ballistic coefficient, which characterizes their braking, increases (Tertyshnikov, 2020). Moreover, the aerodynamic accelerations for a dust particle are two orders of magnitude greater than for a micrometeoroid of a meteor stream with a size, for example, an order of magnitude greater, with the same static stability margin. This causes large fragments of the meteor shower to break ahead, since as dust particle size decreases and the density of dust and micrometeoroids remains the same, their ballistic coefficient is inversely proportional to the cube of their diameter, and their area is proportional to the square of these dimensions. As dust particle mass increases, the sensitivity of their deceleration to variations in the density of the upper atmosphere decreases.

Micrometeoroids smaller than the critical size (~100 micrometers) decelerate above 100 km slowly enough to radiate frictional energy without melting. Therefore, they can reach the Earth's surface. The selection of meteor shower fractions by aerodynamic braking contributes to variations in the observed zenith op-tical density of meteor showers [11]. For larger fractions, which precede the arrival of fine dust, the atmospheric transparency to solar ultraviolet radiation will be higher on the date of the meteor shower's maximum. Furthermore, the long axis of the dust particles rotates perpendicular to the lines of force of the weak magnetic field. The resulting dust conductivity anisotropy in the Earth's electric field contributes to the polarization of transmitted light and the diffraction of solar ultraviolet radiation. Atmospheric thermodynamics also influence variations in the settling density of meteoric dust. The dominant 6-7-day periodicity in variations of the diurnal ESR marker corresponds to the time delay required for the meteor shower to reach its maximum from the turbopause altitude, at a rate of approximately 3 km/day, to the mesopause, where meteoric dust can accumulate due to atmospheric thermodynamic gradients. The accumulation of settling meteoric dust at mesopause altitudes manifests itself in variations in transmitted ultraviolet radiation, affecting the "natural germicidal lamp" mode. Below the mesopause, a layer of anomalous thermodynamic gradients is located at stratopause altitudes, in the ozonosphere, and at the level of the velopause.

These layers also provide conditions for meteoric dust accumulation. However, below 20 km and the Junge layer, terrestrial and cosmic dust actively mix. The influence of meteoric dust on the Chapman cycle of ozone molecule formation and on the ozone layer requires further research, as meteor showers create unique conditions for variations in solar ultraviolet radiation [12]. As an example of this effect, Figure 6 presents "generalized portraits" of the excess and asymmetry coefficients of satellite measurements at a wavelength of 121.6 nm for 2008-2023. The arrow indicates the date of the maxima of strong meteor showers: December 14 (a) and August 13 (b). Day 11 of the time scale falls on the indicated dates of the meteor shower maxima. Day 33 of the time scale in Figure 6a corresponds to January 6 – almost the beginning of the Christmas frosts and the arrival of meteoric dust at the stratopause level, where its spatial distribution is non-uniform. This effect will manifest itself in the thermodynamics and morphology of the ozone layer and below with a delay of several days. The anomalous spike in fragment 6a may be due to the coincidence of a complex of December meteor showers. For the August Perseids in Figure 6b coefficient spikes occur on August 22 and the first ten days of September. By Au-gust 22, meteoric dust crosses the mesopause, and its illumination by solar ultraviolet radiation in the 315-400 nm range reaching the ozonosphere "inhibits" the thermodynamics of the ozonosphere, with subsequent phenomenological effects by the autumnal equinox. These effects will inevitably manifest themselves in blood markers.

## Conclusion

Statistical processing of blood samples from the St. Petersburg Clinical Hospital revealed changes that correspond in time to the dates of strong meteor showers and increases in incoming solar ultraviolet radiation. The dynamics of ESR estimates, which characterize the activity of inflammatory processes, show dominant cyclical patterns with periods of 3-4 and 6-7 days. Similar effects were revealed in the leukocyte and lymphocyte counts, with minima occurring on the dates of meteor shower maxima, dominant periodicities, and strong signals of immune system activation following strong meteor shower maxima.

## References

1. Tertyshnikov A V (2025) Variations in F10.7 by New Dates of Maximum Meteor Streams. Solar System Research 59: 56.
2. Shapovalov S N (2021) Dependence of UVB-UVA Solar Radiation in the 280–400 nm Range on Changes in the Total Magnetic Field of the Sun. Russ Meteorol Hydrol 46: 212-216.
3. Varakin Yu Ya, Ionova V G, Gornostaeva G V, Sazanova E A, Sergienko N P, et al. (2011) The Effect of He-liogeophysical Disturbances on Hemorheological Parameters in Healthy Individuals. Zemsky Vrach 2: 21-24.
4. Komarov F I, Breus T K, Rapoport S I, et al. (1994) Medical and biological effects of solar activity Bulletin of the Rus-sian Academy of Medical Sciences 11: 37-49.
5. Tertyshnikov A V (1999) Seismo-ozone effects and the problem of earthquake prediction. – St. Petersburg: A.F. Mozhaisky VIKU, pp. 197.
6. (1985) Meteoric substance. Spatial distribution model. Moscow: Publishing House of Standards, GOST 25645.128-85, p. 24.
7. Grun E, Zook H A, Fechtig H, Giese R H (1985) Collisional balance of the meteoritic complex. Ica-rus 62: 244-272.
8. Mironov V V, Tolkach M A (2017) Models of the meteoroid environment in near-Earth space and determination of the meteoroid flux density. Space Engineering and Technology 2(17): 49-62.
9. (2005) Space environment (natural and artificial). Model of spatiotemporal distribution of flux density of technogenic substance in outer space. Moscow: Standartinform. GOST: 25645.167-2005, p. 36.
10. Paul Wiegert, Jeremie Vaubaillon, Margaret Campbell-Brown (2009) A dynamical model of the sporadic meteoroid complex. Icarus. Elsevier 201(1): 295-310.
11. Ryabinin I O. UV radiation meter, spectroradiometer, spectrophotometer. AvaSpec-2048 Ultraviolet Radiation Spectrometer.
12. (2024) Meteor_showers.

**ISSN: 2574-1241**

DOI: 10.26717/BJSTR.2026.66.010286

**AV Tertyshnikoy .** Biomed J Sci & Tech Res



**Submission Link**: https://biomedres.us/submit-manuscript.php